

On the Nature of AX J2049.6+2939/AX J2050.0+2914

Emi Miyata^{1,8}, Kouji Ohta², Ken'ichi Torii³, Toshiaki Takeshima^{4,5}, Hiroshi Tsunemi^{1,8},
Takashi Hasegawa⁶, and Yasuhiro Hashimoto⁷

Received _____; accepted _____

¹Department of Earth and Space Science, Graduate School of Science, Osaka University, 1-1 Machikaneyama, Toyonaka, Osaka 560-0043 JAPAN; miyata@ess.sci.osaka-u.ac.jp, tsunemi@ess.sci.osaka-u.ac.jp

²Department of Astronomy, Faculty of Science, Kyoto University, Sakyo-ku, Kyoto 606-8502 JAPAN; ohta@kusastro.kyoto-u.ac.jp

³NASDA TKSC SURP, 2-1-1 Sengen, Tsukuba, Ibaraki 305-8505 JAPAN; Torii.Kenichi@nasda.go.jp

⁴Code 662, NASA Goddard Space Flight Center, Greenbelt, MD 20711, USA; takeshim@ginpo.gsfc.nasa.gov

⁵Universities Space Research Association, 7501 Forbes Blvd., Suite 206, Seabrook, MD 20706, USA

⁶Gunma Astronomical Observatory, Ohtomo, Maebashi, Gunma JAPAN; hasegawa@watarase.astron.pref.gunma.jp

⁷Carnegie Observatories, 813 Santa Barbara Street, Pasadena, CA 91101; hashimot@vorp.al.ciw.edu

⁸CREST, Japan Science and Technology Corporation (JST), 2-1-6 Sengen, Tsukuba, Ibaraki 305-0047 JAPAN

ABSTRACT

AX J2049.6+2939 is a compact X-ray source in the vicinity of the southern blow-up region of the Cygnus Loop supernova remnant (Miyata et al. 1998a). This source was the brightest X-ray source inside the Cygnus Loop observed during the ASCA survey project. The X-ray spectrum was well fitted by a power-law function with a photon index of -2.1 ± 0.1 . Short-term timing analysis was performed and no coherent pulsation was found. Follow-up observations with ASCA have revealed a large variation in X-ray intensity by a factor of $\simeq 50$, whereas the spectral shape did not change within the statistical uncertainties. In the second ASCA observation, we found another X-ray source, AX J2050.0+2941, at the north east of AX J2049.6+2939. During the three ASCA observations, the X-ray intensity of AX J2050.0+2941 varied by a factor of $\simeq 4$. No coherent pulsations could be found for AX J2050.0+2941.

We have performed optical photometric and spectroscopic observations in the vicinity of AX J2049.6+2939 at the Kitt Peak National Observatory (KPNO). As a result, all objects brighter than B -band magnitude of 22 in the error box can be identified with normal stars. Combined with the X-ray results and the fact that there are no radio counterparts, AX J2049.6+2939 is not likely to be either an ordinary rotation-powered pulsar or an AGN. The nature of AX J2049.6+2939 is still unclear and further observations over a wide energy band are strongly required.

As to AX J2050.0+2941, the long-term X-ray variability and the radio counterpart suggests that it is an AGN.

Subject headings: supernova remnants: individual (Cygnus Loop) — X-rays: Spectra — X-rays: Stars — stars: neutron

1. Introduction

Supernovae (SN) with a massive progenitor star leave behind a stellar remnant. A massive star with a mass (M) of $10 M_{\odot} < M < 40 M_{\odot}$ leaves a neutron star while that with a $M > 40 M_{\odot}$ leaves a blackhole. The Cygnus Loop is a well evolved supernova remnant (SNR) and has been widely observed from radio to X-ray wavelengths. Miyata et al. (1998b) investigated the central portion of the Cygnus Loop and concluded that there were Si, S, and Fe rich plasmas in the center of the Loop. Comparing their abundance ratios with the theoretical calculations of nucleosynthesis by a SN explosion, they estimated the progenitor mass of $\sim 25 M_{\odot}$. Furthermore, Miyata et al. (1999) reported a progenitor mass of $\sim 15 M_{\odot}$ based on the radial distribution of heavy elements from the north-eastern region toward the central portion. In both cases, we expect that a neutron star must have been left behind the SN which produced the Cygnus Loop. As mentioned in Miyata et al. (1998a; hereafter paper I), there have been several observations to search for a neutron star associated with the Cygnus Loop. So far, no compact source has been established.

The ASCA Observatory is a powerful tool to discover embedded neutron stars because of its high detection efficiency at hard X-ray region and has discovered more than a dozen neutron stars. We have reported the discovery of a compact X-ray source, AX J2049.6+2939, during the ASCA survey project of the Cygnus Loop (Paper I). Its X-ray properties suggest that it is a neutron star or an active galactic nucleus (AGN). If it is a neutron star, it is definite that the Cygnus Loop must have originated from a massive progenitor star.

In this paper, we performed optical photometric and spectroscopic observations to investigate whether or not it is an AGN. We also performed the timing analysis for follow-up ASCA observations and RXTE observations to investigate the possibility of a neutron star which might associate with the Cygnus Loop.

2. Optical Observations

Because of the possibility that the X-ray source is an AGN, we examined it via optical observations. We performed optical imaging observations of the field containing AX J2049.6+2939 in the B -band and the R -band with the WIYN 3.5m at KPNO in 1997 November. The exposure time was 600 s for each band. The pixel scale was $\simeq 0''.2$. The data were reduced and analyzed in the usual manner with *IRAF*. Photometric calibration was made using Landolt's standard stars (SA 112 and SA 92) (Landolt, 1992) and a photometric error was estimated to be 0.03 mag. The magnitudes of the objects are $R \sim 17 - 20$ mag and $B \sim 19 - 21$ mag with an accuracy of ~ 0.2 mag. Astrometry was made using the *USNO-A1* catalog and the positional error was found to be less than $1''$. The R -band image centered on the X-ray position is shown in figure 1 with an error circle of a radius of $10''$ obtained by the ROSAT HRI (paper I).

If the X-ray source is an AGN, the optical magnitude estimated from the X-ray flux obtained in the first ASCA observation is $B = 17 - 18$ mag by a consideration of the galactic HI column density (paper I). Thus we selected possible optical counterparts as the objects which have a B -band magnitude of $17 - 22$ mag located within the error circle; we extended the possible optical magnitude range to be more secure in the identification. The number of candidates thus selected is four, of which coordinates and magnitudes are listed in table 1. We also added one more object (No. 5) as a candidate for the spectroscopic observation, because it is located very close to the error circle as shown in figure 1. Although we searched for an object behind the bright source in the error circle, no significant object was found. It should be noted that the brightest optical object ($V = 12.6$ mag) in the error circle was identified with a G-type star based on an optical spectroscopy reported in paper I and was excluded from the candidates in this observation.

Optical spectroscopy of the candidates was conducted in 1998 October with the Gold

Camera Spectrograph attached to the KPNO 2.1m telescope. A grating of 158 lines mm^{-1} and an order cut filter of GG400 were used, which gave a spectral coverage of 5000 – 10000Å with a spectral resolution of $\sim 12\text{Å}$. One pixel covered 4.6Å and 0"78. The slit width used was 2" and seeing during the observing run was $\sim 2''$. An exposure time was 20 to 30 min and typically two or three exposures were taken for each object. We used an internal quartz lamp taken just after each exposure as a flat. Data were reduced and analyzed in the usual manner using *IRAF*. The obtained spectrum of No. 1 shows a TiO band feature at around 6160 Å as well as Mg b absorption line and is identified with an M-type star. The spectra of Nos. 2, 3, 4, and 5 show an Mg b absorption and a Na D absorption at $z = 0$, and these objects are identified with stars (presumably G or K stars). The spectral types of identified stars are also consistent with obtained $B - R$ colors. We therefore conclude that there are no AGNs in the expected magnitude range within the error circle.

3. X-ray Observations

3.1. ASCA observations

We performed two follow-up observations with ASCA. (For a detailed description of ASCA, see Tanaka, Inoue, & Holt, 1994). In the following ASCA analysis, we focused on the GIS data since the GIS possesses higher detection efficiency in the hard X-ray band and a high timing resolution below 10 keV (Ohashi et al. 1996; Makishima et al. 1996). The second observation with ASCA was performed on 1998 May 7. We excluded all the data taken at elevation angle below 5° from the night earth rim and 25° from the day earth rim, a geomagnetic cutoff rigidity lower than 6 GV, and the region of the South Atlantic Anomaly. We also applied a “flare-cut” to maximize the signal-to-noise ratio, as described in Ishisaki et al. (Ishisaki Y. et al, 1997, in the ASCA News letter, No.5). The exposure time is $\simeq 25.4$ ksec after the data screening. We constructed three kinds of images for the GIS data

set: a total count image, a non-X-ray background image, and a cosmic X-ray background image. The non-X-ray background image was produced with the H02-sorting method in *DISPLAY45* (the detailed description of this method is in Ishisaki (1996)). The image of the cosmic X-ray background was extracted from the Large Sky Survey (LSS) data (Ueda et al. 1999) acquired during the ASCA PV phase. We also extracted the non-X-ray background image from the LSS data to produce an image of the mean cosmic X-ray background only. In the energy band below 2 keV, the thermal emission from the Cygnus Loop is dominant. Thus, we extracted background-subtracted GIS images in the energy band of 2 – 10 keV shown in figure 2. The X-ray flux of AX J2049.6+2939 is much lower than that of the first observation (paper I). The count rate of AX J2049.6+2939 is $\simeq (3.9 \pm 1.3) \times 10^{-3}$ c s⁻¹/GIS and is a factor of $\simeq 50$ lower than that of the first observation. As clearly seen in figure 2, a bright compact source can be found at the north-eastern direction of AX J2049.6+2939. This source was detected in the first observation but not detected with the ROSAT HRI (see figure 1c in paper I). The location (J2000) of this source is $\alpha = 20^{\text{h}}50^{\text{m}}0^{\text{s}}$ and $\delta = 29^{\circ}41'$ with an error radius of 70". We tentatively call this source as AX J2050.0+2941. Unfortunately, this source is outside of the SIS FOV.

We observed the region in the vicinity of AX J2049.6+2939 again for the third observation. It was performed in 1998 November 10. We screened the data using the same method as for the second observation, giving a total observation time of 7.7 ksec. The image obtained with the GIS is shown in figure 3. The GIS count rate of AX J2049.6+2939 is $(2.4 \pm 2.0) \times 10^{-3}$ c s⁻¹/GIS and is consistent with that of the second observation.

We should note that AX J2049.6+2939 was detected at only a two sigma significance level in the SIS data.

3.1.1. X-Ray Spectra of AX J2049.6+2939

We extracted the X-ray spectrum of AX J2049.6+2939 and the background spectrum from the same region in the same manner as for the first observation (described in paper I). We made spectra both from the GIS2 and GIS3 data and added them together. The response matrix was created from a count-weighted sum of GIS2 and GIS3 responses. The cross-calibration uncertainties are less than 5 % as may be found at the [ASCA GOF web page](#). We applied several simple models to our data set and the results are described in table 3. N_{H} is fixed to $3.1 \times 10^{21} \text{cm}^{-2}$ which is the same value as that obtained in the first observation (paper I). We should note that the fitting results were not affected when we chose the other values that we obtained in table 1 of paper I. In all models listed in table 3, we obtained consistent results with those of the first observation within statistical uncertainties. Therefore, the spectral shape seems to be unchanged whereas the flux was decreased by a factor of $\simeq 50$.

3.1.2. X-Ray Spectra of AX J2050.0+2941

We next extracted the X-ray spectrum of AX J2050.0+2941 for all three data sets. As shown in fig 1 (b) in paper I, AX J2050.0+2941 is severely contaminated by AX J2049.6+2939. The point spread function (PSF) of the ASCA XRT has a sharp core with a broad wing structure (Serlemitsos et al. 1995). Although there are complex structures in the PSF, the on-axis PSF shows a well-defined axially symmetric shape. The $7'$ off-axis PSF shows a small elongation along the tangential direction but is still axially symmetric, as shown in figure 5b of Serlemitsos et al. (1995). We observed AX J2049.6+2939 and AX J2050.0+2941 within $7'$ from the on-axis for all three observations. Therefore, we select the region which is on the opposite side of AX J2050.0+2941 across the location of AX J2049.6+2939 to accumulate the background spectrum. The count rates of AX

J2050.0+2941 are $(1.3 \pm 0.2) \times 10^{-2} \text{ c s}^{-1} / \text{GIS}$, $(9 \pm 2) \times 10^{-3} \text{ c s}^{-1} / \text{GIS}$, and $(3 \pm 2) \times 10^{-3} \text{ c s}^{-1} / \text{GIS}$ for the first, second, and third observations, respectively. We applied the same models as those for AX J2049.6+2939 and the results are given in table 4. In the third observation, we could not obtain meaningful results due to low X-ray intensity and relatively short exposure time. Only bremsstrahlung and power-law models are acceptable for both data sets. We found no difference in their spectral shapes within the statistical uncertainties. In the case of the power-law model, the X-ray flux in the energy range of 2 – 10 keV is $(3.4 \pm 0.6) \times 10^{-13}$ and $(3.9 \pm 0.6) \times 10^{-13} \text{ erg s}^{-1} \text{ cm}^{-2}$ for the first and the second data sets, respectively. In the third observation, we calculated the X-ray flux assuming the power-law model with a photon index of -2.25 and N_{H} of $1.0 \times 10^{22} \text{ cm}^{-2}$ to be $(9 \pm 4) \times 10^{-14} \text{ erg s}^{-1} \text{ cm}^{-2}$. AX J2050.0+2941 shows the X-ray intensity variation by a factor of 4.

We obtained the Einstein IPC data set in the vicinity of AX J2050.0+2941 from the HEASARC/GSFC Online Service using the observation ID of 3782. Unfortunately, AX J2050.0+2941 is located just on the support grid of IPC and it is difficult to estimate the X-ray flux with a high degree of accuracy. The ROSAT HRI also observed the region of AX J2050.0+2941 as the sequence number of 500462. However, it was not detected above the 5 σ level. This might be consistent with the fact that the obtained N_{H} value was high. Thus, we could not investigate the long-term X-ray intensity variation for AX J2050.0+2941.

3.1.3. Short-Term Variation

We searched for short-term intensity variations of the two compact sources in the second observation using the GIS data. Since we assigned the timing bit of the GIS to be 10 for the ASCA second and third observations, the timing resolutions for high and medium bit rate are 61 and 488 μs (Ohashi et al. 1996). We used the data obtained both with the high

and the medium bit rate for the temporal analysis. After applying the barycentric correction on photon arrival times, we performed the FFT analysis with a Nyquist frequency of 1024 Hz. We found no coherent pulsations for neither AX J2049.6+2939 nor AX J2050.0+2941. The 99 % upper limits on the pulsed fraction for the sinusoidal pulse shape are 42 % and 36 % for 0.7 – 10 keV band and 62 % and 55 % for 2 – 10 keV band, respectively, in the second observation.

Because the Fourier transform method is not sensitive enough for non-sinusoidal pulse shapes, we also tried the epoch folding search method. Arrival times were folded into 10 phase bins for assumed trial periods. The epoch folding method is extremely time consuming on the computer and we restricted our search to the period range of $5 \text{ s} < P < 1000 \text{ s}$. No significant pulsation was detected. Upper limits of pulse amplitude (99 % confidence) were obtained as 23 % (0.7–10 keV) and 44 % (2–10 keV) for AX J2049.6+2939 and 21 % (0.7–10 keV) and 41 % (2–10 keV) for AX J2050.0+2941, respectively.

To further examine the aperiodic variations, we extracted light curves of 0.7–10 keV with the bin sizes of 512, 1024, 2048, and 4096 s for the two sources. No significant aperiodic variations were found at the 99 % confidence level. In these timescales, the rms noise was found to be 26 % and 20 % for AX J2049.6+2939 and AX J2050.0+2941, respectively. These results show that there is no excess variation above the Poisson error.

Due to poor statistics, we could not obtain a meaningful result for the third data set.

3.2. RXTE observation

AX J2049.6+2939 was observed with RXTE on 1997 December 22-23. RXTE carries three scientific instruments: the Proportional Counter Array (PCA), the High-Energy X-Ray Timing Experiment (HEXTE), and the All-Sky Monitor (ASM). Detailed description

of RXTE can be found in Bradt, Rothschild, and Swank (1993). Here we analyze the data from the PCA which consists of five collimated (1° FWHM) proportional counter units (PCUs) that contain three multianode detector layers with a mixture of xenon and methane gas (Jahoda et al. 1996).

To maximize the signal-to-noise ratio between 2 and 10 keV (5 – 27 PH channel), we accumulated photon events from the top xenon/methane layer of the PCA. We excluded all the data taken at elevation angle below 10° from the earth rim, the region from the South Atlantic Anomaly (SAA) to within 30 min after the end of the SAA passage, and the period when there was severe electron contamination (`ELECTRON0`, `ELECTRON1`, `ELECTRON2` ≥ 0.1). Since PCU-3 was switched off for some part of our observation, we ignored PCU-3 data to maximize the observation time. This yields a total integration time of $\simeq 26$ ks.

We constructed light curves for the 2 – 10 keV band with 64, 128, and 512 s binning and estimated the background for each time bin using `pcabackest` with a background model of `pca_bkgd_faint17_e3v19990824.mdl` and `pca_bkgd_faint240_e3v19990909.mdl` retrieved from the GSFC ftp site. There is no variability in the X-ray flux during the observation. The rms noise is 69, 64, and 64 % for the 64, 128, and 512s binned data. These results show that there is no excess variation above the Poisson error. The mean count rate is 0.53 ± 0.06 c s $^{-1}$ /4PCU.

We estimated the contamination from the shell emission of the Cygnus Loop. We extracted the ASCA 2–5 keV image with the same method as Miyata et al. (2000), removed the region with the radius of $4'$ centered on AX J2049.6+2939, and estimated the intensity of shell emission there based on the region shown in Fig 1-a in paper I. We obtained the collimator response file for the RXTE from the calibration database (CALDB) supported by GSFC (`p0coll_96jun05.fits`) and convolved it with the processed ASCA image. Thus, we estimated the RXTE countrate of the shell emission of the Cygnus Loop

to be $\sim 0.3 - 1 \times 10^{-3} \text{ c s}^{-1} / 4\text{PCU}$ assuming the plasma temperature ranges from 0.3–0.8 keV (Miyata 1996). Therefore, the contamination of thermal emission can be negligibly small.

As mentioned in section 3.1, we found a hard X-ray compact source, AX J2050.0+2941, near AX J2049.6+2939. AX J2050.0+2941 shows X-ray variability by a factor of 4. Since the angular separation is less than $7'$, both sources were simultaneously observed with RXTE. Assuming the X-ray flux of AX J2050.0+2941 to decrease linearly from the first to the second observation, the X-ray flux of AX J2050.0+2941 at the RXTE observation phase can be estimated to be $1.1 \times 10^{-12} \text{ erg s}^{-1} \text{ cm}^{-2}$. We assumed the X-ray spectrum of AX J2049.6+2939 to be a power-law spectrum with a photon index of -2.1 and N_{H} to be $3.1 \times 10^{21} \text{ cm}^{-2}$ (paper I), resulting in the X-ray flux of AX J2049.6+2939 to be $(3 \pm 2) \times 10^{-13} \text{ erg cm}^{-2} \text{ s}^{-1}$. We should note that we take into account the 20 % cross calibration uncertainties between ASCA and RXTE. This value is an order of magnitude lower than that of the ASCA first observation and is similar to that of the second ASCA observation.

We have performed a FFT analysis for the frequency range of 10^{-3} –500 Hz on the barycenter corrected time series data of 2–10 keV detected in the top xenon/methane layer. No significant coherent pulsation was found. The poor signal to noise statistics due to the relatively low X-ray flux and high background rate ($\gtrsim 95$ % of the total counts) did not allow us to constrain the better upper limit of the coherent pulsations than those with the first and second ASCA observations.

We also tried the epoch folding search method for the RXTE data in the same way as that for ASCA. Although we searched for the period range $5\text{s} < P < 1000\text{s}$, the χ^2 values were found to become large for the period range $P > 20 \text{ s}$ due to the time variable background counts. We therefore restricted the search range to $5\text{s} < P < 20\text{s}$. An upper

limit of pulse amplitude was found to be $\sim 70\%$ of the estimated source count rate of AX J2049.6+2939.

3.3. Long-Term X-ray Variation of AX J2049.6+2939

We constructed the long-term light curve of AX J2049.6+2939, using the Einstein IPC, the ROSAT HRI, RXTE PCA, and ASCA GIS data, which span a period of 19 years. For the IPC and HRI observations, we extracted the count rate of AX J2049.6+2939 while the background count rate was estimated from regions where the intensity of thermal emission from the Cygnus Loop was similar to that of AX J2049.6+2939. We assumed a power-law function and took into account the error regions obtained in paper I to calculate the X-ray flux. Figure 4 shows the obtained long-term light curve of AX J2049.6+2939. We find that the X-ray flux of AX J2049.6+2939 generally decreases during 19 years while a “flare event” occurred during the first ASCA observation.

We should note that the X-ray variability shown in figure 4 contains a lot of uncertainties: insufficient (or no) cross calibration, different energy bands, assumed model and N_{H} . However, we can still confirm a large X-ray intensity variation with the ASCA data, solely.

4. Discussion

4.1. Identification of AX J2050.0+2941

AX J2050.0+2941 shows an X-ray intensity variation of a factor of 4 during the ASCA observations. It shows no short-term variability. The X-ray spectrum of AX J2050.0+2941 can be fitted by a power-law function with a photon index of $\simeq -2.2$ or a thermal

bremsstrahlung with kT_e of 3 keV.

As mentioned in paper I, radio emission was detected in the vicinity of AX J2050.0+2941 using *Skyview* supported by HEASARC/GSFC. Williams et al. (1992) analyzed both radio-loud and radio-quiet quasars with Ginga in the energy range of 2 – 20 keV and found a correlation between the radio-loudness and the X-ray spectral index. The X-ray spectra of radio-loud and radio-quiet quasars were well represented with a power-law function with an index of ~ -2.0 and ~ -1.6 , respectively. Since we have found a radio counterpart of AX J2050.0+2941, it is likely to be a radio-loud quasar. If AX J2050.0+2941 is an AGN, the reddening-corrected optical magnitude estimated from the X-ray flux is $17 \lesssim B \lesssim 21$ mag (Zamorani et al. 1981). We then checked for a counterpart in optical wavelengths using the *USNO-A1* catalog. However, AX J2050.0+2941 is detected only in the ASCA observation and the error circle is relatively large ($70''$). More than forty objects were found within the error circle. We therefore need further X-ray observations of AX J2050.0+2941 with Chandra or XMM-Newton to determine the position of AX J2050.0+2941 with high accuracy for its identification.

4.2. Identification of AX J2049.6+2939

We have found a long-term X-ray variability of over 19 years for AX J2049.6+2939. Only in the sequence of ASCA observations, AX J2049.6+2939 shows a long-term X-ray variability with a factor of $\simeq 50$ but no short-term X-ray variability. The X-ray spectrum can be fitted by a power-law function with an index of $\simeq -2.3$ or a thermal bremsstrahlung with kT_e of 4 keV for three observations. Such a large X-ray variability suggests that it is not likely to be an ordinary rotation-powered pulsar but it could be an AGN.

We have performed optical photometric and spectroscopic observations in the vicinity

of AX J2049.6+2939 and found no AGNs within its error circle. Thus, we conclude that AX J2049.6+2939 is not likely to be an AGN.

We should note, however, that we performed the optical photometric observations in 1997 November where the expected X-ray flux might be lower than that of the ASCA first observation. We can estimate the X-ray flux of AX J2049.6+2939 at 1997 November to be $\simeq 2 \times 10^{-12}$ erg s $^{-1}$ cm $^{-2}$ from figure 4 assuming a smooth decrease of the X-ray flux from the ASCA first observation to the ASCA second observation. The optical magnitude expected from this value is $B = 17 - 19$ mag (Zamorani et al. 1981). We have investigated five objects within the error circle whose B -band magnitude range 17 – 22 mag based on WIYN observations. So, even if the X-ray flux is lower than our estimate, we can conclude that no AGNs are found within the error circle.

We investigated the possibility of the G-type star considering our new X-ray observations. The X-ray spectrum of the G-type star is well represented by an isothermal, two-temperature, or DEM (differential emission measure) thermal model. The kT_e values range from $\simeq 80$ eV to $\simeq 2.5$ keV and abundances of heavy elements are roughly solar values (Güdel et al 1997). The kT_e value and abundances of AX J2049.6+2939 are a little higher and much lower, respectively, than those of G-type stars if we apply a thin thermal model (paper I). For these stars, flares with much larger luminosities have been observed where kT_e and emission measure becomes larger than those of quiescent state. However, the timescales of their flare are roughly several tens of minutes or hours which is much shorter than ‘flare event’ seen in figure 4. Therefore, we again conclude that AX J2049.6+2939 is not likely to be a G-type star.

It is well known that the X-ray pulsar 1E 2259+586 in the supernova remnant G109.1–1.0 shows a flux variation of a factor of a few on timescales of a few years (Corbet et al. 1995). This pulsar belongs to a member of anomalous X-ray pulsars (AXPs).

Members of this group have several common properties including a relatively long pulse period of 6 – 12 s and a steep X-ray spectrum characterized by a power-law function with a photon index of $-2.5 \sim -4$. Comparing these characteristics, long-term X-ray variability seems to be too large for AXPs, there is no coherent pulsation, and the spectrum is flatter than those of AXPs. Thus, AX J2049.6+2939 is not likely to be an AXP.

A remarkably similar situation is found for the compact source, 1E 161348-5055, in the supernova remnant RCW 103. Gotthelf, Petre & Vasisht (1999) reported the X-ray variability of 1E 161348-5055. They found that its X-ray flux decreased by an order of magnitude over a period of 18 years. No coherent pulsation has been detected from this source (Gotthelf et al 1999 and references therein). These characteristics are similar to those of AX J2049.6+2939 whereas the X-ray spectrum of 1E 161348-5055 is much softer than that of AX J2049.6+2939. They propose that 1E 161348-5055 is either a cooling neutron star (but less plausible), an advection dominated accretion flow (ADAF) around a blackhole, or an AXP. If we apply the same analogy for AX J2049.6+2939, this source might well be accreting through an ADAF. Since there are CO molecular clouds at the western edge of the Cygnus Loop (Scoville et al. 1977), such a model might be applicable to AX J2049.6+2939. The X-ray spectra of AX J2049.6+2939 are consistent with that expected from the ADAF model (Narayan, Barret, & McClintock 1997; Manmoto, Mineshige, & Kusunose 1997). The ADAF model also predicts that the shape of the X-ray spectrum is independent of the X-ray flux. Thus, there is no definite evidence for ADAF but apparent X-ray features are consistent with those expected from the ADAF model.

5. Conclusion

We performed wide-band spectroscopic observations in the vicinity of AX J2049.6+2939. Based on the optical photometric and spectroscopic observations, we can rule out the

possibility of an AGN. AX J2049.6+2939 shows a large X-ray variability over 19 years, which excludes the possibility of an ordinary rotation-powered pulsar. Thus, the ADAF model would be a plausible one, although no definite evidence is obtained. As calculated by Narayan, Barret, & McClintock (1997) and Manmoto, Mineshige, & Kusunose (1997), the spectrum generated by ADAF shows the synchrotron peak which comprises the Rayleigh-Jeans slope and the optically thin synchrotron emission in the radio regime. The Comptonization of the synchrotron photons leads to one or two peaks from IR to UV regimes. In the X-ray and γ ray regimes, the bremsstrahlung emission plus photons suffering multiple Compton scattering and emission from saturated Comptonized photons are dominant. Therefore, further simultaneous observations over a wide energy band are essential to investigate its nature.

We have found another hard X-ray emitting compact source, AX J2050.0+2941, which is in a direction north-eastern from AX J2049.6+2939. We also found radio (4850MHz) emission in the vicinity of AX J2050.0+2941. Due to its large error circle, we found more than forty objects for the optical candidate of AX J2050.0+2941. We therefore need further X-ray observations in the vicinity of AX J2050.0+2941 with Chandra or XMM-Newton in order to determine its position more accurately. It would be essential to investigate the relationship with the Cygnus Loop.

We thank Profs. S. Kitamoto, F. Nagase, and S. Mineshige for invaluable comments and suggestions. We appreciate Mr. C. Baluta for careful reading of manuscript. We thank *ASCA-ANL* and *DISPLAY 45* developing team members, especially Dr. Ishisaki. Part of this research has made use of data obtained through the High Energy Astrophysics Science Archive Research Center Online Service, provided by the NASA/Goddard Space Flight Center. This research is partially supported by ACT-JST Program, Japan Science and Technology Corporation.

REFERENCES

- Asai K., Dotani T., Mitsuda K., Hoshi R., Vaughan B., Tanaka Y., Inoue H. 1996, PASJ, 48, 257
- Bradt H. V., Rothschild R. E., Swank J.H. 1993, A&AS, 97, 355
- Bradt H.D.V, McClintock J.E. 1983, ARA&A. 21, 13
- Gotthelf E.V., Petre R., Vasisht G. 1999, ApJ. 514, L107
- Güdel M, Guinan E.F., Skinner S.L. 1997, ApJ, 483, 947
- Ishisaki Y. 1996, Ph.D. thesis of Univ. of Tokyo, ISAS RN 613
- Jahoda K., Swank J.H., Giles A.B., Stark M.J., Strohmayer T., Zhang W., Morgan E.H. 1996, Proc. SPIE, 2808, 59
- Landolt, A.U. 1992, AJ, 104, 340
- Lasker B.M., Sturch C.R., McLean B.J., Russell J.L., Jenkner H., Shara M.M. 1990, AJ, 99, 2019
- Lochner J.C., Roussel-Dupré D. 1994, ApJ, 435, 840
- Narayan R., Barret D., McClintock J.E. 1997, ApJ, 482, 448
- Makishima K., Tashiro M., Ebisawa K., Ezawa H., Fukazawa Y., Gunji S., Hirayama M., Idesawa E. et al. 1996, PASJ, 48, 171
- Manmoto T., Mineshige S., Kusunose M. 1997, ApJ, 489, 791
- Mitsuda K., Inoue H, Nakamura N., Tanaka Y. 1989, PASJ, 41, 97

- Miyata E., Tsunemi H., Torii K., Hashimoto-dani K., Tsuru T., Koyama K., Ayani K., Ohta K., Yoshida M. 1998a, PASJ, 50, 475 (paper I)
- Miyata E. 1996, PhD thesis, Osaka University (ISAS RN 591)
- Miyata E., Tsunemi H., Kohmura T., Suzuki S., Kumagai S. 1998b, PASJ, 50, 257
- Miyata E., Tsunemi H. 1999, ApJ, 525, 305
- Miyata E., Tsunemi H., Koyama K., Ishisaki Y. 2000, Adv. Space. Res. 25, 555
- Ohashi T., Ebisawa K., Fukazawa Y., Hiyoshi K., Horii M., Ikebe Y., Ikeda H., Inoue H. et al. 1996, PASJ, 48, 157
- Scoville N.Z. et al. 1997. ApJ, 216, 320
- Serlemitsos P.J. et al. 1995, PASJ, 47, 105
- Tanaka Y., Inoue H., Holt S.S. 1994, PASJ, 46, L37
- Turner T.J., Pounds K.A. 1989, MNRAS, 240. 833
- Ueda Y., Takahashi T., Inoue H., Tsuru T., Sakano M., Ishisaki Y., Ogasaka Y., Makishima K. et al. 1999, ApJ, 518, 656
- Williams O.R. et al. 1992, ApJ, 389, 157
- Zamorani G., et al. 1981, ApJ, 245, 357

Table 1. Optical photometry for counterpart candidates of AX J2049.6+2939

Designation	Right Ascension (J2000)	Declination (J2000)	<i>B</i> -mag	<i>R</i> -mag
No.1	20 ^h 49 ^m 34 ^s 84	29° 38' 53''8	22.0	19.6
No.2	20 ^h 49 ^m 35 ^s 01	29° 38' 48''7	21.0	19.2
No.3	20 ^h 49 ^m 35 ^s 24	29° 38' 41''8	20.9	19.6
No.4	20 ^h 49 ^m 36 ^s 02	29° 38' 49''5	20.9	19.7
No.5	20 ^h 49 ^m 36 ^s 05	29° 38' 43''9	18.9	17.0

Table 2. ASCA Observations

Pointing	Sequencer Number	Date	GIS exposure time [ks]
1st	55026080	1997 June 03	7.6
2nd	56036000	1998 May 07	25.7
3rd	56036010	1998 Nov 10	7.7

Table 3. Fitting results of AX J2049.6+2939

Model	AX J2049.6+2939		
	Parameter	Normalization	χ^2 / d.o.f
Blackbody	$kT_e = 0.7 \pm 0.2$ keV	$(1.1^{+0.2}_{-0.3}) \times 10^{-35}$ erg s ⁻¹ ^a	22.1 / 33
Bremsstrahlung	$kT_e = 3.3^{+4.6}_{-1.5}$ keV	$4^{+2}_{-1} \times 10^{-2}$ cm ⁻⁶ pc	19.6 / 33
Power law	$\Gamma = -2.5^{+0.5}_{-0.7}$	$(9^{+6}_{-4}) \times 10^{-5}$ photons keV ⁻¹ cm ⁻² ^b	20.3 / 33

Note. — Quoted errors are at 90 % confidence level.

^aDistance to the source is assumed to be 770 pc.

^bFlux is shown at 1 keV.

Table 4. Fitting results of AX J2050.0+2941

Model	First observation				Second observation			
	Parameters	N_{H} ^a	Normalization	χ^2 / d.o.f	Parameters	N_{H} ^a	Normalization	χ^2 / d.o.f
Blackbody	0.7 ± 0.1 keV	$\lesssim 4$	$(2.8_{-0.5}^{+0.7}) \times 10^{-33}$ ^b	38.0 / 27	1.0 ± 0.2 keV	$\lesssim 3$	$(2.6 \pm 0.5) \times 10^{-35}$ ^b	54.6 / 40
Bremsstrahlung	2_{-1}^{+2} keV	5_{-3}^{+5}	15_{-6}^{+16} ^c	35.2 / 27	$\gtrsim 4$ keV	$\lesssim 8$	$(5.7_{-0.8}^{+3.3}) \times 10^{-2}$ ^c	47.6 / 40
Power law	$\Gamma = -2.9_{-0.9}^{+0.6}$	9_{-5}^{+7}	$4_{-2}^{+7} \times 10^{-2}$ ^d	35.6 / 27	$\Gamma = -1.6_{-0.8}^{+0.4}$	$\lesssim 11$	$8_{-4}^{+17} \times 10^{-5}$ ^d	47.9 / 40

Note. — Quoted errors are at 90 % confidence level.

^a N_{H} is in unit of 10^{21} cm^{-2} .

^bDistance to the source is assumed to be 770 pc and luminosity is shown in unit of erg s^{-1} .

^cEmission measure is shown in unit of cm^{-6} pc.

^dFlux at 1 keV is shown in unit of photons $\text{keV}^{-1} \text{cm}^{-2}$.



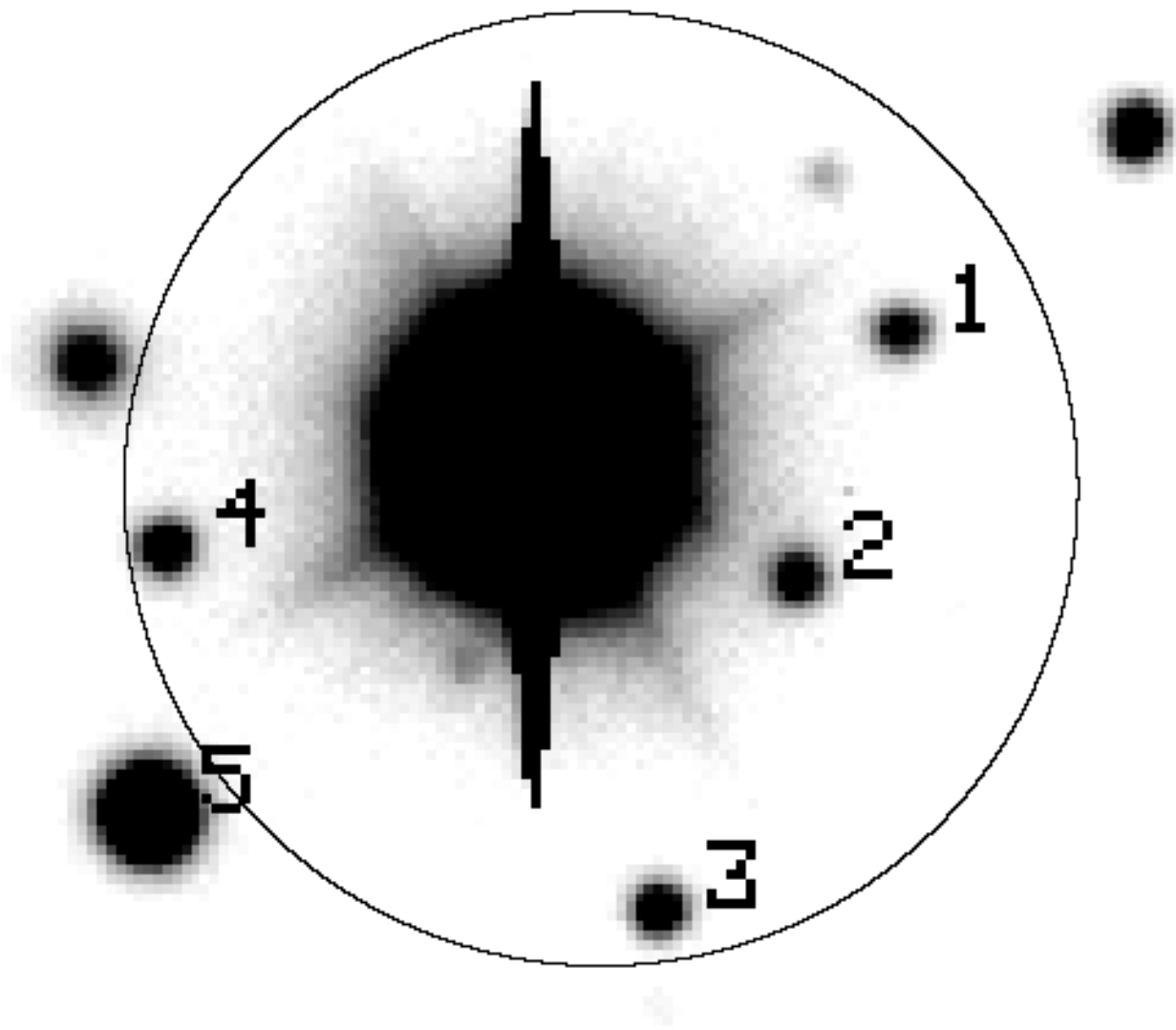
FIGURE CAPTIONS

Fig. 1.— Optical (R -band) finding chart for counterpart candidates. North is to the top, and east is to the left. Coordinates of the candidates are listed in Table 1. Error circle for the X-ray source is shown with a radius of $10''$.

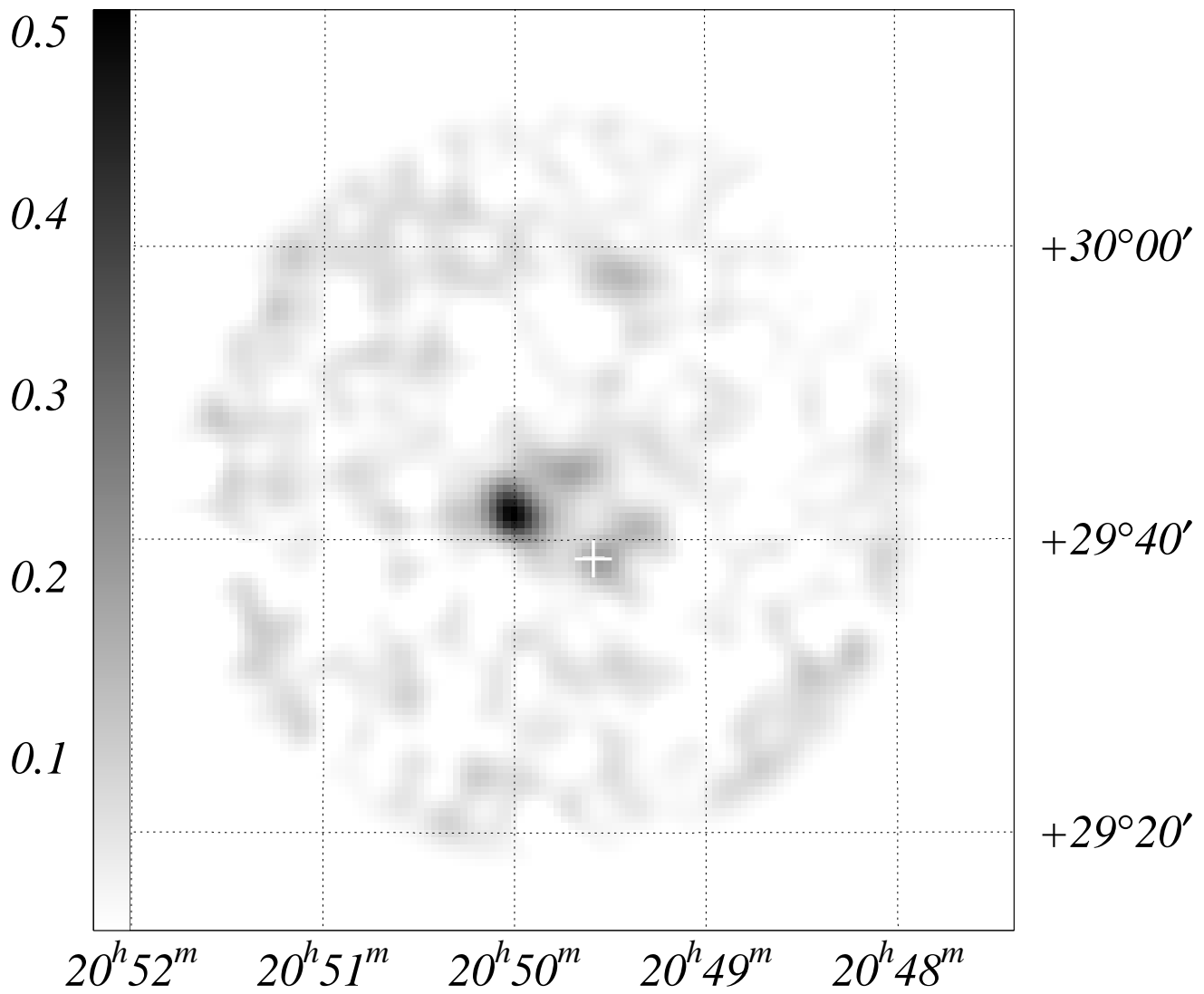
Fig. 2.— Background-subtracted GIS image in the energy band of $2 - 10$ keV in the second observation of AX J2049.6+2939. The image was smoothed with a Gaussian function of $\sigma = 1'$. The location of AX J2049.6+2939 is marked with a white cross.

Fig. 3.— Same as figure 2 but for the third observation.

Fig. 4.— Long-term X-ray variability of AX J2049.6+2939.



$x10^{-3} \text{ c/s/arcmin}^2$ *2nd Observation*



3rd Observation

